Large-scale chemical dissection of mitochondrial function

Bridget K Wagner[1,5], Toshimori Kitami[1,2,5], Tamara J Gilbert[1], David Peck[1], Arvind Ramanathan[1], Stuart L Schreiber[1], Todd R Golub[1,3] & Vamsi K Mootha[1,2,4]

Mitochondrial oxidative phosphorylation (OXPHOS) is under the control of both mitochondrial (mtDNA) and nuclear genomes and is central to energy homeostasis. To investigate how its function and regulation are integrated within cells, we systematically combined four cell-based assays of OXPHOS physiology with multiplexed measurements of nuclear and mtDNA gene expression across 2,490 small-molecule perturbations in cultured muscle. Mining the resulting compendium revealed, first, that protein synthesis inhibitors can decouple coordination of nuclear and mtDNA transcription; second, that a subset of HMG-CoA reductase inhibitors, combined with propranolol, can cause mitochondrial toxicity, yielding potential clues about the etiology of statin myopathy; and, third, that structurally diverse microtubule inhibitors stimulate OXPHOS transcription while suppressing reactive oxygen species, via a transcriptional mechanism involving PGC-1α and ERRα, and thus may be useful in treating age-associated degenerative disorders. Our screening compendium can be used as a discovery tool both for understanding mitochondrial biology and toxicity and for identifying novel therapeutics.

Oxidative phosphorylation (OXPHOS) is the core mitochondrial pathway responsible for ATP synthesis. The OXPHOS system consists of $\sim$90 protein components, including all 13 of the proteins that are encoded by the mitochondrial genome (mtDNA)[1]. On time scales of seconds to minutes, mitochondrial ATP synthesis is regulated primarily by substrate availability and allosteric control[2]. During growth and development, however, transcription and translation of OXPHOS genes are carefully orchestrated between the nuclear and mitochondrial genomes to achieve sustained, metabolic adaptation. Over 50 mutations in the mtDNA and nuclear genome have been linked to rare, but devastating, inborn errors of OXPHOS metabolism[3]. Moreover, quantitative declines in OXPHOS activity and efficiency have been linked to nearly all age-associated degenerative diseases, including type 2 diabetes mellitus[4–6]. Hence, understanding OXPHOS function and regulation, particularly within the context of the entire cell, has important implications for managing many human diseases.

Traditional approaches to studying energy metabolism in the mitochondrion have focused either on the kinetics of ATP synthesis in isolated mitochondria or on transcriptional control of mitochondrial components. For instance, classic bioenergetic studies that assessed the effects of chemical inhibitors on isolated mitochondria[2] focused on the acute regulation of mitochondrial activity, ignoring the cell's ability to respond and adapt over longer time scales. Many of the chemical reagents used in these studies were incompatible with cellular or whole-animal studies, making it difficult to extend their relevance *in vivo*. More recently, molecular studies have shed light on the transcriptional control of OXPHOS[7], although relatively little is known about how these regulatory programs are coupled to other cellular processes.

Our goal was to combine physiologic and genomic profiling of intact cells in order to probe OXPHOS function and regulation in response to thousands of small-molecule perturbations. A systematic mapping between physiology and gene expression may shed light on how the nuclear genome and mtDNA are coordinated under different cellular conditions to maintain energy homeostasis. Large-scale approaches based on perturbing cells have been used successfully to study cell growth[8], gene expression[9,10] and tumorigenesis[11], but no previous studies appear to have combined cell-based, physiological readouts with genomic profiling. Our integrated approach provides a richer description of cellular mitochondrial state, reporting on more stable changes in the organelle, which can be useful for studying its longer-term adaptations.

Here, we report the construction of a mitochondrial screening compendium and its application to problems in mitochondrial biology, drug toxicity and therapeutics. Our compendium is freely available and should provide a framework for understanding how the activity and regulation of mitochondrial OXPHOS are integrated within the context of the entire cell.

RESULTS
Systematic profiling of OXPHOS physiology and transcription
We developed high-throughput assays in 384-well format for cell viability, mitochondrial physiology and gene expression (**Fig. 1**, Methods). We used differentiated C2C12 murine myotubes, a cell

[1]Broad Institute of Massachusetts Institute of Technology and Harvard, Seven Cambridge Center, Cambridge, Massachusetts 02142, USA. [2]Center for Human Genetic Research, Massachusetts General Hospital, 185 Cambridge Street, Boston, Massachusetts 02114, USA. [3]Department of Pediatric Oncology, Dana-Farber Cancer Institute, 44 Binney Street, Boston, Massachusetts 02115, USA. [4]Department of Systems Biology, Harvard Medical School, 200 Longwood Avenue, Boston, Massachusetts 02446, USA. [5]These authors contributed equally to this work. Correspondence should be addressed to V.K.M. (vamsi@hms.harvard.edu).
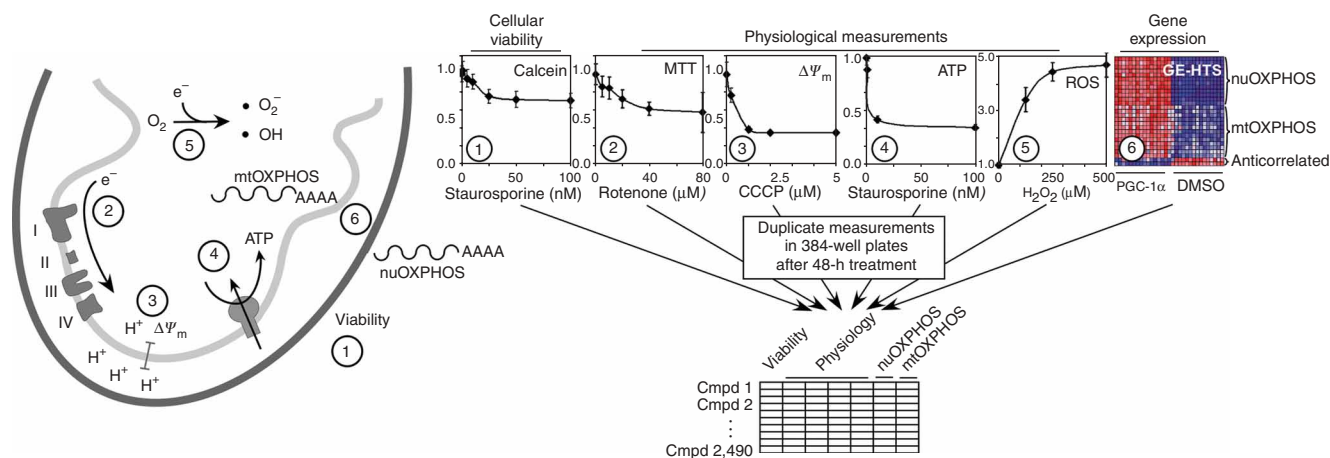
Figure 1 Complementary profiles of viability, mitochondrial physiology and gene expression across 2,490 chemical perturbations. The calcein assay (1) measures cell viability and filters out overtly toxic compounds, such as staurosporine. The MTT assay (2) measures cellular dehydrogenase activity, which is inhibited by the complex I inhibitor rotenone. The JC-1 assay (3) measures the mitochondrial membrane potential ($\Delta\Psi_m$) and drops acutely after the addition of the mitochondrial uncoupler carbonyl cyanide m-chlorophenylhydrazone (CCCP). A luciferase-based assay measures ATP (4), which is reduced by staurosporine. CM-H$_2$DCFDA is a fluorescent probe of cellular ROS (5), which can be stimulated by the addition of H$_2$O$_2$. The expression of both nuOXPHOS and mtOXPHOS transcripts is measured by a multiplex PCR technique, GE-HTS (6). Each column of the heat map represents one sample replicate; expression levels for each gene are row-normalized. Treatment with PGC-1α, an inducer of OXPHOS gene expression, is used as a positive control. All assays were performed in biological duplicate in 384-well format after 48 h of treatment in differentiated murine C2C12 myotubes. Data from 2,490 distinct compounds are incorporated into the screening compendium.

line that has been used extensively to study mitochondrial biogenesis and bioenergetics[12]. We measured cell viability using a calcein dye[13] and monitored mitochondrial physiology by probing four parameters related to OXPHOS. These included the JC-1 assay, which measures mitochondrial membrane potential ($\Delta\Psi_m$)[14]; the MTT ((3-(4,5-dimethylthiazol-2-yl)-2,5-diphenyltetrazolium bromide)) assay, which measures mitochondrial dehydrogenase activity[15]; a luciferase-based assay for cellular ATP levels[16]; and a fluorescent probe (CM-H$_2$DCFDA, (5-(and-6)-chloromethyl-2′,7′-dichlorodihydrofluorescein diacetate), which measures reactive oxygen species (ROS), a by-product of OXPHOS[17] (see Methods). We also developed an immunofluorescence-based assay for cytochrome c protein content (see Methods).

To complement these physiological assays, we also performed gene expression–based high-throughput screening (GE-HTS)[18,19] to profile transcripts associated with nuclear and mtDNA OXPHOS (see Methods). GE-HTS is a facile, high-throughput method that quantifies dozens of transcripts simultaneously. It is a multiplexed PCR strategy that combines ligation-mediated amplification with multicolored bead detection to identify and quantify transcripts of interest (see **Supplementary Fig. 1** online). We adapted GE-HTS to profile simultaneously all 13 mtDNA-encoded OXPHOS (mtOXPHOS) transcripts as well as 12 nuclear-encoded OXPHOS (nuOXPHOS) transcripts (**Supplementary Fig. 1**). These 12 nuOXPHOS transcripts include representatives from all five OXPHOS protein complexes and were selected because they capture virtually all of the variation in gene expression shown by the entire OXPHOS repertoire, as assessed by analysis of over 5,000 genome-wide microarrays (data not shown). Of note, our GE-HTS assay also monitored transcripts that tend to be anticorrelated to OXPHOS expression or are invariant across many conditions as assessed by microarray assays, and thereby assist in data analysis (see Methods). Together, our GE-HTS assay faithfully 'tags' the expression of the entire OXPHOS system. Moreover, because the expression of OXPHOS genes is so highly correlated, measuring
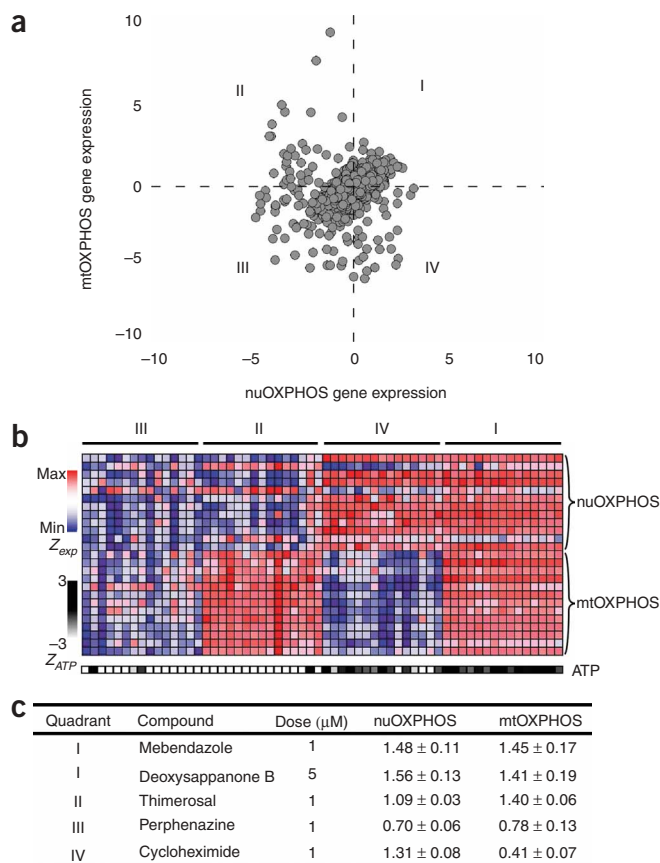
multiple transcripts increases the signal-to-noise ratio with which we can detect subtle effects of individual compounds[4].

We performed the viability, physiology and gene-expression assays in duplicate in differentiated C2C12 myotubes following 48-h treatment with each of 2,490 compounds. Our chemical library consists of known bioactives, two-thirds of which are marketed drugs. Using a scoring algorithm dependent upon the distribution of mock-treated (DMSO) wells[20,21], we arrived at a normalized score for each assay in each well (**Supplementary Table 1** online). In our compendium, we have included data from our screen for cytochrome c protein expression, though we excluded it from subsequent analyses owing to the high coefficient of variation. Correlation analysis indicated that our remaining readouts (one for viability, four for OXPHOS physiology and one for OXPHOS gene expression) provide complementary information (**Supplementary Fig. 2** online).

The resulting compendium is freely available to the public and is useful for dissecting mitochondrial function (**Supplementary Table 1**). Unlike traditional approaches for studying mitochondrial function, it enables us to track systematically how changes in nuclear and mitochondrial OXPHOS gene expression are coupled to mitochondrial physiology over thousands of perturbations. We used this approach to explore three problems focused on mitochondrial biology, drug toxicity and the identification of novel therapeutics.

Cross-talk between nuclear and mitochondrial genomes

First, we used the compendium to identify the cellular signals involved in coordinating nuclear OXPHOS (nuOXPHOS) and mtDNA OXPHOS (mtOXPHOS) transcription. Expression of OXPHOS genes from the two genomes must be tightly coupled to maintain energy homeostasis in the mitochondrion[22,23]. Moreover, although OXPHOS expression can change in human diseases, it is often unclear whether the changes are primary or reactive and how these changes relate to cellular physiology[4,24–26]. We therefore focused on the relationship between nuOXPHOS and mtOXPHOS transcripts across

Figure 2 Coupling of nuclear and mitochondrial OXPHOS expression. (**a**) A two-dimensional plot of the composite Z-scores for nuOXPHOS and mtOXPHOS expression is shown. (**b**) Row-normalized heat map displaying the top 15 compounds in each quadrant (I–IV). Heat map of nuOXPHOS and mtOXPHOS expression is shown along with ATP levels. (**c**) Real-time PCR validation of select compounds at the indicated doses, using *Atp5a1* (nuOXPHOS) and *mt-Co1* (mtOXPHOS) normalized to *Hprt1* (internal control). Values indicate average fold change from mock-treated (DMSO) wells ± s.d. in four biological replicates.

believed to be caused by ubiquinone depletion, which can block electron transport[28]. However, clinical and epidemiological studies of the association between statins and myopathy have produced conflicting results[28]. Of the six statins present in our screening collection, three (fluvastatin, lovastatin and simvastatin) produced strong decreases in cellular ATP levels and MTT activity (**Fig. 3a**). Previous studies showed that lovastatin and simvastatin reduce MTT activity and ATP levels[29], consistent with our high-throughput screening results. To eliminate the possibility that we uncovered two classes based merely on potency, we measured cellular ATP levels over doses ranging up to 40 μM. We observed the same segregation of effects, with atorvastatin, pravastatin and rosuvastatin showing little to no effect on cellular or mitochondrial ATP levels (**Supplementary Fig. 3** online).

To determine whether this profile might represent a signature of drug-induced myopathy, we established a centroid profile for the three mitochondria-active statins (fluvastatin, lovastatin and simvastatin) and sought to identify other clinically used drugs with a similar assay profile. The ten nearest-neighbor drugs to the centroid statin profile (**Fig. 3b**) were amoxapine, cyclobenzaprine, propranolol, griseofulvin, pentamidine, paclitaxel, propafenone, ethaverine, trimeprazine and amitriptyline. Notably, five of these compounds (amoxapine, propranolol, griseofulvin, pentamidine and paclitaxel) have also been associated with skeletal muscle myopathy or myalgia[30–34], a strikingly high proportion in comparison to the small fraction of all FDA-approved drugs believed to be associated with this side effect[35]. This suggests that the drug profile might be indicative of myopathy or myalgia. Further examination of the screening data revealed that two electron transport chain inhibitors—β-dihydrorotenone (a complex I inhibitor) and antimycin A (a complex III inhibitor)—were among the 16 nearest-neighbor compounds to this assay profile, which provides mechanistic insight into this profile. Together, the data support the idea that myopathy induced by these five other drugs could be mitochondrial in origin.

We were struck by the fact that one of these nearest-neighbor drugs is propranolol, a widely used antihypertensive agent. Follow-up experiments confirmed that propranolol, but not other selective β1 blockers, decreases cellular ATP levels in a dose-dependent manner (**Supplementary Fig. 3**). Because many patients take both a statin and a β-blocker for cardioprotection, we were curious whether the two drugs might interact to cause toxicity. We thus assessed cellular ATP levels after treatment with all possible combinations of the six statins in our collection and three β-blockers (atenolol, metoprolol and propranolol), with all concentrations falling between 2.5 and 10 μM (**Fig. 3c**). Although neither atenolol nor metoprolol showed an effect either alone or in combination with any statin, propranolol had an additive effect on statin-induced decrease in ATP levels, as determined using the Bliss independence model (**Fig. 3c**)[36]. Our screening compendium and follow-up experiments (**Fig. 3c**) thus raise the potentially important hypothesis that patients on a combination of propranolol and one of the three statins (fluvastatin, lovastatin, simvastatin) might be at a higher risk for developing myopathy or myalgia.
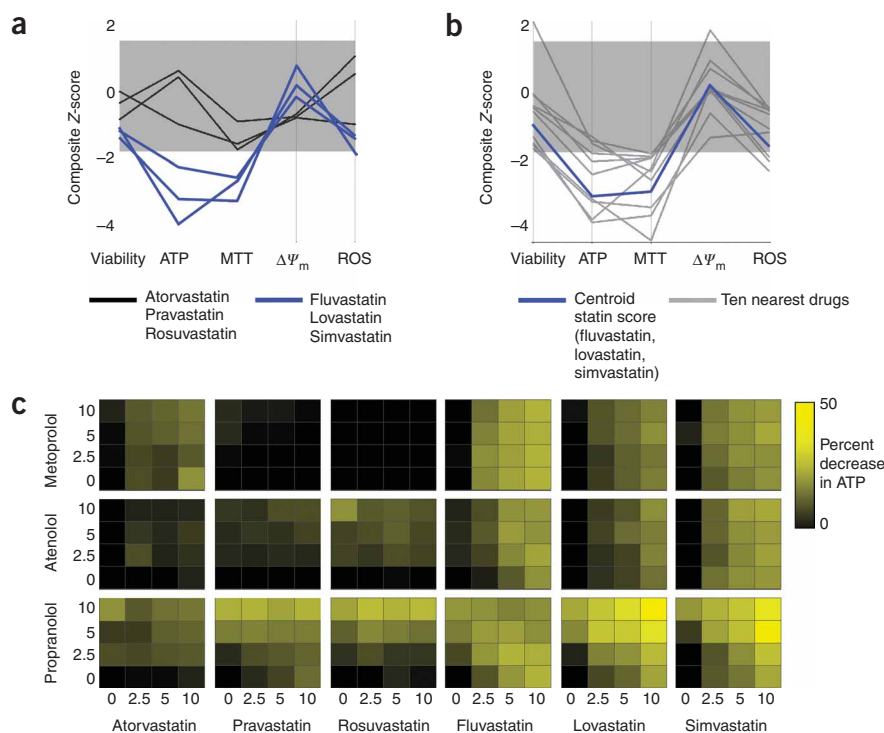
the chemical perturbations. As expected, the majority of compounds influence the two sets of genes in a coordinated manner (**Fig. 2a**). However, we identified some compounds that decouple the coordination between these two genomes (**Fig. 2b** and **Supplementary Table 2** online), a subset of which we confirmed with follow-up dose response curves and RT-PCR analysis (**Fig. 2c**). Specifically, we discovered that the eukaryotic protein synthesis inhibitors emetine, anisomycin and cycloheximide preferentially increase nuOXPHOS expression, implying that translational control might be important in coordinating the two genomes. Follow-up studies revealed that 1 μM cycloheximide elevated nuOXPHOS 1.3-fold but decreased mtOXPHOS 2.4-fold (**Fig. 2c**). Notably, we found that nuOXPHOS expression, but not mtOXPHOS expression, correlated strongly with cellular ATP levels (**Fig. 2b**). To determine whether nuOXPHOS expression drives the changes in ATP levels, or reacts to changes in ATP levels, we performed follow-up time-course analyses with 20 μM perphenazine, a compound that decreased nuOXPHOS expression. Whereas nuOXPHOS expression declined significantly (21%, *t*-test, $P = 0.004$) within the first hour of treatment, cellular ATP levels remained unchanged (0.6%, *t*-test, $P = 0.84$) at these early time points. At later time points, however, ATP levels dropped significantly (8 h: 11% decrease, *t*-test, $P = 1.4 \times 10^{-5}$, 24 h: 27% decrease, *t*-test, $P = 6.3 \times 10^{-22}$), suggesting that the decline in nuOXPHOS expression precedes and drives the decline in cellular ATP levels.

Exploring the mitochondrial basis for drug toxicity
To probe the role of mitochondria in human drug toxicity, we focused on the statins—3-hydroxy-3-methylglutaryl–coenzyme A (HMG-CoA) reductase inhibitors taken by nearly 100 million patients worldwide. Statins are associated with a 0.1–0.5% incidence of myopathy[27],

Figure 3 Statin-induced mitochondrial toxicity. (a) Six of the HMG-CoA reductase inhibitors (statins) in clinical use are in the chemical screening collection. Composite Z-scores for cell viability, ATP generation, MTT activity, $\Delta\Psi_m$, ROS levels and gene expression are shown, where negative scores indicate a decrease in signal compared to mock-treated (DMSO) wells. The gray shading indicates scores that fall within the noise envelope. (b) A centroid statin score was generated by calculating the arithmetic means of the composite Z-scores for fluvastatin, lovastatin and simvastatin. The ten nearest-neighbor clinically used drugs (amoxapine, cyclobenzaprine, propranolol, griseofulvin, pentamidine, paclitaxel, propafenone, ethaverine, trimeprazine and amitriptyline) were identified by calculating the root-mean-square distance of each performance vector to the profile of interest. (c) All six statins were tested in combination with three clinically used β-adrenergic blockers (propranolol, atenolol and metoprolol) for their effects on cellular ATP levels. Compound concentrations are indicated on each axis, and the color indicates the change in ATP levels (ranging from black, for no change, to yellow, for a 50% decrease). Data represent the average of six independent replicates; coefficients of variation were all below 15%.

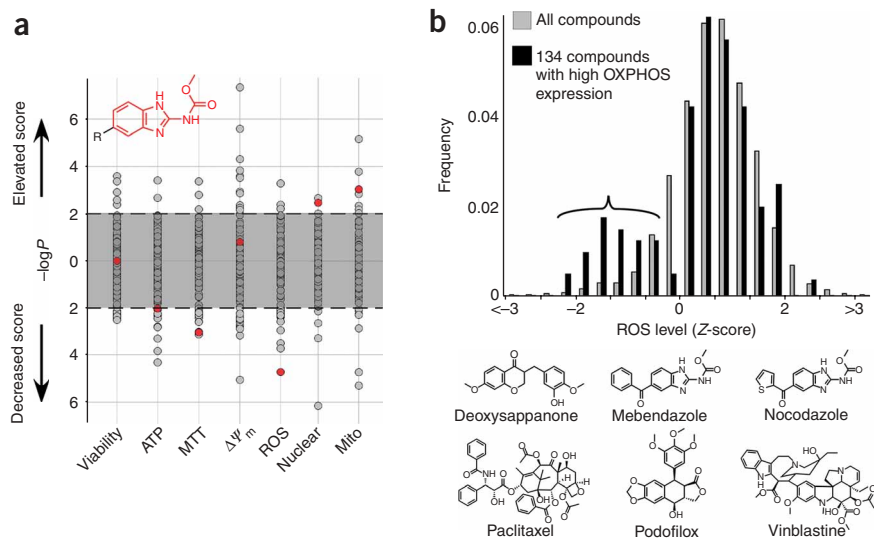## Discovering lead compounds for common degenerative diseases

Finally, we searched for lead compounds that might hold therapeutic potential for common human diseases. As we and others have recently shown that a decline in OXPHOS gene expression and an elevation in ROS generation are associated with type 2 diabetes[4,37,38], neurodegeneration[39] and aging[5,6], we queried our compendium to identify compounds that might be capable of elevating OXPHOS expression while reducing ROS accumulation.

We used two computational strategies to spotlight such compounds (see Methods). First, we developed a simple analytical strategy to determine whether any structurally related set of compounds might boost OXPHOS expression while also suppressing ROS accumulation (**Supplementary Table 3** online). This strategy involves organizing all compounds based on structural similarity (Methods) and then asking whether members of a cluster had concordant scores in a given assay (**Fig. 4a**). The advantage of this strategy is that individual compounds might show a subtle response not detectable in a primary screen with duplicate measurements, whereas the grouped analysis provides added statistical power. Second, in a complementary approach, we sought to identify individual compounds that promote OXPHOS gene

Figure 4 Two complementary strategies to identify small molecules that boost OXPHOS gene expression and decrease ROS levels. (a) Mining the compendium for sets of structurally related compounds that achieve the desired activity. All compounds were organized into 624 clusters based on the chemical descriptors molecular weight, log P, number of hydrogen bond donors and acceptors, and number of rotatable bonds. The Mann-Whitney rank-sum statistic for each cluster and each assay was then calculated. The significance of each cluster in each assay is shown, with points above zero indicating positive composite scores and points below zero showing negative composite scores. A nominal P = 0.01 is delimited by the dashed lines. The red data points spotlight a single cluster that is significant for the desired activity, with the shared chemical scaffold shown. (b) Mining the compendium for individual compounds that achieve the desired activity. The distributions of ROS scores are shown for all compounds (gray) and for compounds associated with the highest OXPHOS gene expression (black). The latter follow a bimodal distribution, and the smaller mode (bracketed) contains six compounds that elevate OXPHOS expression and decrease ROS levels, with chemical structures shown.

expression while reducing ROS levels. The advantage of this method is that it can reveal structurally unrelated compounds that individually exert large effect sizes in the two assays of interest. We focused on the upper tail of the combined nuclear and mitochondrial OXPHOS gene-expression distribution (**Fig. 4b**).

Notably, both analytical strategies spotlighted microtubule modulators, including both a microtubule stabilizer (paclitaxel) and several destabilizers (mebendazole, nocodazole, podophyllotoxin and vinblastine), as agents that boost OXPHOS expression while suppressing ROS levels. The second strategy also yielded deoxysappanone B, a natural product found in sappan wood[40], whose molecular mode of action is unknown and has not been previously linked to microtubule biology. The other microtubule inhibitors within the compound collection (colchicine and griseofulvin) did not display the same decrease in ROS levels, but did show a modest increase in OXPHOS expression.

Next, we were interested in confirming these primary screening results and determining whether the effects on OXPHOS expression and ROS levels occur via shared or distinct mechanisms, and whether these were on-target or off-target effects of microtubule disruption. We therefore retested the microtubule modulators at a range of 20 nM to 20 μM (**Fig. 5a**). Treatment with either deoxysappanone B, mebendazole, nocodazole, podophyllotoxin or vinblastine increased OXPHOS expression and decreased ROS levels at the same dose of 2 μM. In contrast, paclitaxel showed effects in the two assays at 20 nM, suggesting a shared mechanism for OXPHOS expression and ROS level. Notably, at these doses, these compounds did not decrease cell viability (**Fig. 5a**), indicating that the decline in ROS is not simply a reflection of overt cytotoxicity. We also imaged tubulin immuno-fluorescence after treatment with deoxysappanone B and paclitaxel, two compounds that showed distinct potencies. For both compounds, the potency required for microtubule disruption was the same as that
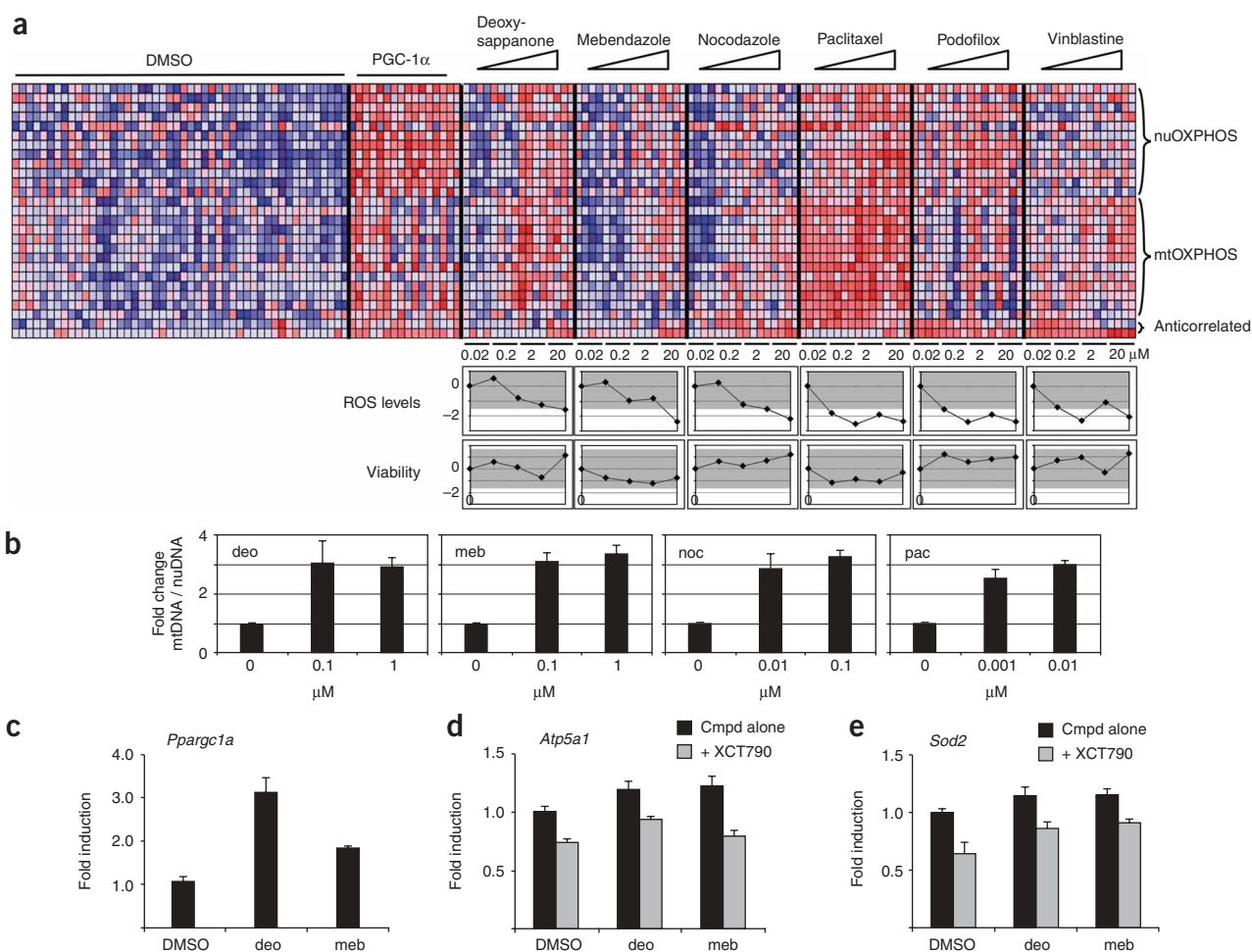

Figure 5 Secondary analyses of the effects of microtubule inhibitors on OXPHOS gene expression and physiology. (**a**) Compounds indicated in **Figure 4b** were retested at 20 nM, 200 nM, 2 μM and 20 μM. Gene expression levels are represented as a row-normalized heat map, with negative controls (DMSO treatment) and positive controls (PGC-1α treatment) shown. Dose-response curves for ROS levels and viability are also provided, where the *y*-axis is the composite *Z*-score. Shaded area indicates the noise envelope ($P > 0.05$). Data shown are the results of four biological replicates per concentration. (**b**) Analysis of mtDNA/nuDNA copy number ratio after treatment with four of the compounds (deo, deoxysappanone B; meb, mebendazole; noc, nocodazole; pac, paclitaxel), using three biological replicates, normalized to DMSO treatment alone. (**c**) Quantitative PCR measurement of *Ppargc1a* gene expression, in response to either DMSO alone, 5 μM deoxysappanone B (deo) or 1 μM mebendazole (meb). (**d**) Quantitative PCR measurement of the nuclear OXPHOS gene *Atp5a1*. Cells were either treated with compound alone (black bars) or in combination with 5 μM of the ERRα inverse agonist XCT790 (gray bars). (**e**) Quantitative PCR measurement of *Sod2*, which encodes the ROS scavenger MnSOD, as in **d**. Means and s.d. of expression data are the result of four biological replicates.

required to affect OXPHOS expression and ROS levels (**Supplementary Fig. 4** online). To our knowledge, deoxysappanone B has not previously been linked to microtubule inhibition, but it now has been predicted to do so and the prediction has been validated by this study. Given that structurally and mechanistically diverse microtubule modulators increased OXPHOS gene expression, decreased cellular ROS and disrupted microtubules with equivalent potencies, it is likely that these effects are directly related to inhibition of microtubules, and not due to an off-target effect.

Because mtDNA replication and transcription are often coupled[41], we sought to determine whether any of these compounds promoted mtDNA replication. At the concentrations tested, several of these microtubule modulators—but not podophyllotoxin or vinblastine—increased mtDNA copy number approximately threefold (**Fig. 5b**).

We sought to determine the transcriptional mechanism by which microtubule inhibition might promote OXPHOS expression and mtDNA replication while suppressing ROS. We hypothesized that these changes might be occurring via PGC-1α, a transcriptional coactivator that regulates mitochondrial biogenesis in muscle[42] and whose transcriptional program is diminished in type 2 diabetes[4]. Consistent with this hypothesis, both mebendazole and deoxysappanone B induced the expression of *Ppargc1a* (which encodes PGC-1α) by approximately threefold (**Fig. 5c**). We have previously shown that the transcription factor ERRα serves as a key transcriptional partner of PGC-1α to drive OXPHOS expression in muscle, and that disruption of ERRα with the selective inverse agonist XCT790 suppresses PGC-1α–induced OXPHOS expression[43]. Therefore, we tested whether XCT790 is capable of inhibiting compound-induced transcription. We observed that both mebendazole and deoxysappanone B increased the expression of a nuclear OXPHOS gene, *Atp5a1*, by ∼20%, and that the increase by mebendazole was blunted by XCT790 (**Fig. 5d**), further suggesting a PGC-1α–dependent mechanism of compound activity. The mitochondrial ROS scavenger MnSOD is downstream of the same PGC-1α pathway[44], and as we observed decreased cellular ROS levels after treatment with these small molecules, we also tested the effects of the compounds on this gene. A similar increase in MnSOD levels, which was only partially suppressible by XCT790, was observed with these compounds (**Fig. 5e**). These results suggest that microtubule modulators both activate OXPHOS transcription and reduce cellular ROS levels in a manner involving PGC-1α and ERRα.

DISCUSSION

The mitochondrion is an extremely complex organelle, with components derived from both the nuclear and mitochondrial genomes, whose activity must be carefully coupled to cellular metabolism and signaling. We systematically investigated mitochondrial function using multiple physiological and multiplexed gene-expression assays for OXPHOS following chemical perturbations. The gene-expression and physiological assays provided complementary information and were jointly useful in interpreting the effects of compound treatment. The compendium is freely available and can be used to investigate the network properties of the mitochondrion. Moreover, because so many of the 2,490 compounds tested are well characterized, they can be used immediately to study mitochondrial biology, as illustrated by the three applications we have demonstrated.

First, we focused on how the nuclear genome and mtDNA are coordinated across a variety of physiological states. As this is the first compendium to interrogate the expression of both the nuclear genome and mtDNA, we could show that the bulk of compounds coordinately regulate expression from both genomes. However, similar to the demonstration that the calcium ionophore A-23187 can elevate

nuOXPHOS while decreasing mtOXPHOS[45], we found that eukaryotic protein synthesis inhibitors disrupt cross-talk between these two genomes. We now have an array of chemical tools (**Fig. 2**) to investigate whether protein synthesis inhibitors also disrupt the nuclear-to-mitochondrial genome cross-talk via known pathways or through one or more novel mechanisms.

Second, we mined the compendium to learn about drug toxicity. Our focus on statins revealed a bimodal response from these HMG-CoA reductase inhibitors (**Fig. 3**), with three compounds (atorvastatin, pravastatin and rosuvastatin) forming a group with no activity in our physiological assays and three other compounds (fluvastatin, lovastatin and simvastatin) forming a group showing signs of OXPHOS inhibition. Statins block the synthesis of cholesterol—a precursor to ubiquinone, a mobile electron carrier in the mitochondrion that is critical to OXPHOS function. It has therefore been previously suggested that statin myopathy may result from a respiratory chain blockade[28]. Our data suggest that the statins fluvastatin, lovastatin and simvastatin should be examined further for their effects on skeletal muscle ubiquinone and drug-induced myopathy. Using the statin toxicity signature (**Fig. 3a**), we also discovered that propranolol, a widely used antihypertensive agent, shares the same profile of mitochondrial inhibition. β1-selective blockers such as atenolol and metoprolol, however, did not show this pattern of toxicity (**Supplementary Fig. 3**). The additive interaction we reveal between the statins and propranolol suggests that patients taking both statins and propranolol might be at increased risk for developing skeletal muscle myopathy or myalgia. Because many patients with heart disease are likely to be on this drug combination, our hypothesis can be tested easily and may help to account for the conflicting reports on skeletal muscle myopathy associated with statins.

Third, we queried our compendium for compounds that could potentially reverse signatures associated with age-associated degenerative diseases. We and others have recently reported that a decline in OXPHOS expression and a rise in ROS levels accompany a number of common degenerative diseases, including diabetes, neurodegeneration and aging[4–6,37–39]. Using two computational approaches to mine our compendium, we discovered that structurally unrelated microtubule modulators with diverse mechanisms of action (both stabilizers and destabilizers) increased OXPHOS expression and decreased cellular ROS. Follow-up dose-response studies of mitochondrial function and microtubule disruption suggest that these drugs affect OXPHOS expression and ROS levels via an on-target mechanism.

Our studies raise the possibility that manipulation of the microtubule pathway may reverse the gene-expression and ROS signatures associated with common degenerative diseases and that these may represent therapeutic targets. Previous clinical case reports support this hypothesis. Type 1 and type 2 diabetics treated for parasitic worm infections with mebendazole unexpectedly showed improvement both in fasting blood glucose levels and nonesterified fatty acid metabolism[46]. Blood glucose levels improved without weight loss, suggesting that the improvement in diabetes was not due to a toxic side effect of mebendazole. Moreover, deoxysappanone B, a natural product found in sappan wood, has been reported to be an antidiabetic component of Chinese herbal medicine, although its mechanism was unclear[40]. Our data convincingly demonstrate that deoxysappanone B disrupts microtubules (**Supplementary Fig. 4**).

At a molecular level, we have uncovered an unexpected link between microtubule disruption and an increase in PGC-1α/ERRα–mediated OXPHOS gene expression. Although changes in mitochondrial staining and morphology have been associated with microtubule inhibitors[47], no studies have specifically documented their effects on

OXPHOS expression and ROS levels. It is intriguing to speculate that perhaps interactions between the cytoskeleton and the mitochondrion are important in integrating cellular homeostasis throughout the cell cycle. As many of these microtubule modulators are used for treating cancer, our results may enhance understanding of the metabolic basis of chemotherapeutic action.

Building on decades of research in bioenergetics that yielded a detailed, mechanistic understanding of OXPHOS in isolated mitochondria[48], our screening compendium provides a foundation for understanding how OXPHOS physiology and regulation are integrated within the broader signaling and metabolic network of the cell. Each small-molecule probe modulates a different aspect of cell biology, and our compendium provides insights into how OXPHOS responds to these perturbations by remodeling at the levels of physiology and gene expression. Because many of the small molecules used in this study are well-characterized bioactives, our compendium provides a rich chemical toolkit for manipulating mitochondria in cells and whole animals in a defined manner. Given the growing number of rare and common diseases associated with different types of mitochondrial dysfunction, we anticipate that our compendium will serve as a generic tool for systematically investigating mitochondrial pathogenesis and for restoring mitochondrial function.

METHODS

Cell culture. C2C12 myoblasts (ATCC) were grown in Dulbecco's Modified Eagle's Medium (DMEM, Mediatech) supplemented with 10% (vol/vol) FBS and antibiotics (100 μg/ml penicillin/streptomycin mix) in a humidified atmosphere at 37 °C with 5% CO$_2$. Differentiation into myotubes was induced at 80% density on 'day 0' by changing the medium to DMEM supplemented with 2% (vol/vol) horse serum.

Cell-based high-throughput screening. For all screening, 4,000 C2C12 myoblasts per well were seeded into either black or white 384-well optical-bottom plates (Nunc) at 50 μl per well. On day 4 of differentiation, 100 nl of each compound was pin-transferred in duplicate into fresh medium with a steel pin array, using the CyBi-Well robot (CyBio). To increase the number of mock-treated wells included in the control distribution, we added an additional plate containing DMSO alone. Compound-treated plates were incubated at 37 °C for 48 h. All cell-based assay measurements were performed using the EnVision plate reader (PerkinElmer). The coefficient of variation for each of these assays was estimated to be less than 15%. All data has been deposited in ChemBank: http://chembank.broad.harvard.edu/assays/view-project.htm?id=1000453.

Calcein viability assay. Medium was aspirated from plates, and 30 μl per well 1 μM calcein-AM (Molecular Probes) in phenol red–free medium was added. Plates were incubated for 1 h at 37 °C and washed three times with 50 μl per well PBS. Fluorescence was measured at excitation and emission wavelengths (ex/em) of 485 nm/530 nm.

JC-1 mitochondrial membrane potential assay. Upon depolarization, the JC-1 dye is converted from a diffuse green form to red fluorescent J-aggregates. The ratio of red to green fluorescence serves as a readout of the mitochondrial membrane potential. Medium was aspirated from plates, and 20 μl per well 3.25 μM JC-1 (Molecular Probes) in phenol red–free medium was added. Plates were incubated for 2 h at 37 °C and washed three times with 50 μl per well PBS. Fluorescence was measured first at ex/em 530 nm/580 nm ('red') and then at ex/em 485 nm/530 nm ('green').

Assay for cellular ATP levels. 20 μl per well CellTiterGlo reagent (Promega) was added to 20 μl per well of cell culture medium. Plates were agitated for 2 min and incubated for 10 min at room temperature (22–24 °C) before luminescence was measured.

MTT assay. Medium was aspirated from plates, and 50 μl per well 0.5 mg/ml MTT in phenol red–free medium was added. Plates were incubated for 2 h at 37 °C, and this was followed by aspiration of MTT solution, addition of 50 μl per well DMSO to dissolve formazan crystals, and incubation at 37 °C for 30 min. After incubation, plates were equilibrated to room temperature for an additional 20–30 min. Absorbance was measured at 540 nm.

Reactive oxygen species assay. Medium was aspirated from plates, and 20 μl per well 10 μM CM-H$_2$DCFDA (Molecular Probes) in phenol red–free medium was added. Plates were incubated for 1 h at 37 °C and washed three times with 50 μl per well PBS. Fluorescence was measured at ex/em 485 nm/530 nm.

Cytochrome c protein detection. Cells were fixed with 3.7% (vol/vol) formaldehyde in PBS for 30 min and then washed with TBS containing 0.1% (vol/vol) Tween-20 (TBST) and blocked with TBST + 3% (wt/vol) BSA for 1 h at room temperature. Cytochrome *c* was detected by incubating the cells with primary antibody (Cell Signaling Technology; 1:100) overnight at 4 °C, washing three times with TBST, and incubating with secondary antibody (Alexa Fluor 488–conjugated anti–mouse IgG, Invitrogen; 1:250) for 1 h at room temperature. Plates were washed three times with TBST and fluorescence measured at ex/em 485 nm/530 nm.

Gene expression–based high-throughput screening. We adapted the GE-HTS assay to monitor both nuclear and mtDNA OXPHOS transcripts. To narrow down the list of potential genes from nearly 80 nuclear OXPHOS genes, we used a list of highly co-regulated OXPHOS genes[4] that are coordinately expressed across tissues and are downstream of the PGC-1α transcriptional coactivator. From this list, we selected genes that showed the highest signal-to-noise ratio in the microarray analysis of PGC-1α overexpression in C2C12 myotubes[43] representing all five OXPHOS complexes. We also selected two genes that are downregulated by PGC-1α with the best signal-to-noise ratio. As controls, we selected genes that showed the lowest signal (no treatment effect) and lowest noise (biological variation) in the PGC-1α overexpression data[43], as well as genes previously found to be invariant from the analysis of multiple microarray datasets[49]. We selected control genes that span a wide range of expression levels to prevent biasing for abundant transcripts. The selected OXPHOS transcripts capture the bulk of the variation exhibited by the OXPHOS transcripts represented on over 5,000 publicly available mouse microarrays on the Affymetrix platform (data not shown).

From the list of OXPHOS genes and control genes for GE-HTS, we designed probe pairs with T7 and T3 universal primer sites, 40-bp target sequence split into two 20-bp sequences for each probe, and gene-specific barcode sequence attached to the 5′ probe according to the published assay specification[19]. We selected 40-bp gene-specific target sequences that are not alternatively spliced using oligonucleotide sequences found in the Mouse Exonic Evidence-Based Oligonucleotide Chip (MEEBO, http://alizadehlab.stanford.edu/). Full primer sequences are included in **Supplementary Table 4** online.

The GE-HTS assay was performed as previously described[50]. Because this assay measures the final amount of PCR products rather than providing a real-time measurement of gene expression, we adjusted the parameters in the original protocol so that the abundance of PCR products were within the linear range of the assay. We removed 20 μl of medium and added 25 μl of lysis buffer per well of a 384-well plate, and used 24 PCR cycles instead of the 29 cycles described[50]. We used 32 DMSO-treated and 32 PGC-1α adenovirus–treated wells per 384-well compound plate, with one additional control plate containing 192 DMSO-treated wells, 32 GFP adenovirus–treated wells and 160 PGC-1α adenovirus–treated wells. The PGC-1α adenovirus–treated cells serve as a positive control for increased OXPHOS gene expression, as previously reported[4].

Tubulin immunofluorescence. On day 4 of differentiation, C2C12 myotubes were treated with each compound for 48 h and then fixed for 5 min in ice-cold 100% methanol. Cells were washed once in 50 μl PBSTB2 (PBS with 0.1% (vol/vol) Tween-20 and 2% (wt/vol) BSA) and blocked in PBSTB2 for 1 h at room temperature or overnight at 4 °C. Cells were incubated with an anti-α-tubulin (Sigma-Aldrich) antibody, 1:1,000 in PBSTB2, for 1 h at room temperature, and then washed three times with PBSTB2. Cells were incubated with secondary antibody (Alexa 488–conjugated anti-mouse antibody, 1:500 in PBSTB2) (Molecular Probes) and Hoechst 33342 for 1 h at room temperature and then washed three times in PBSTB2. Cells were visualized using an automated microscope (IX-Micro, Molecular Devices).

Quantitative PCR of mtDNA and transcripts. *mtDNA quantification.* Mitochondrial DNA copy number was assessed by quantifying the abundance of the

mitochondrial gene *mt-Co1* (encoding cytochrome *c* oxidase 1) relative to the nuclear gene *Actb* (encoding β-actin). DNA from cells were extracted using DNeasy (Qiagen) and quantified for *mt-Co1* and *Actb* copy number using quantitative PCR (Applied Biosystems). The change in the *mt-Co1/Actb* ratio between the compound-treated and DMSO control cells represents the fold change in mtDNA copy number.

Gene expression. We extracted RNA using an RNeasy kit (Qiagen) and synthesized cDNA using a high-capacity cDNA reverse transcription kit (Applied Biosystems) with random hexamers, as described by the manufacturer. The cDNA was then used for real-time PCR quantification of products for mouse *Atp5a1* (Mm00431960_m1), *Sod2* (*MnSOD*; Mm01313000_m1) and *Ppargc1a* (Mm00447183_m1), with *Hprt1* (Mm03024075_m1) serving as an internal control, using TaqMan gene-expression assays (Applied Biosystems).

Statistics. *Cell-based screening.* Composite *Z*-scores reflecting compound performance as compared to a mock-treated (DMSO) distribution were calculated as described[20,21] (see also http://chembank.broad.harvard.edu/details.htm?tag=Help#screeningData).

GE-HTS. We first eliminated wells that failed the assay reaction by filtering out wells in which the raw expression value of *Rps2* (a control gene) was 2 s.d. below the median DMSO control value for each plate. We normalized for plate-to-plate variation by scaling the per-well expression level of each gene to the median expression level of that gene in PGC-1α control wells on each plate. We set the median PGC-1α−treated expression value for each gene to 1, and then normalized for well-to-well variation by dividing the expression level of each OXPHOS gene by the average value of eight control genes for each well. This number represents the processed data value.

To score the expression levels of 12 nuclear- and 13 mitochondrial-encoded OXPHOS genes, we first weighted each gene by its ability to distinguish DMSO control wells from PGC-1α-treated wells. We calculated the signal-to-noise ratio[49] of each gene using our PGC-1α-treated positive control and DMSO negative control, and multiplied the expression value of each gene per well by this signal-to-noise ratio. We then summed these weighted scores over nuclear-encoded or mitochondrial-encoded OXPHOS genes to derive one score each for expression within each genome. Composite *Z*-scores were calculated as described above.

Similarity between assay profiles. We used the cell-based composite *Z*-scores from the ATP, MTT, JC-1 and ROS assays to calculate the root-mean-square distance between performance vectors, as this statistic gives greater weight to values far from zero. We obtained centroid statin scores by taking the arithmetic mean of the composite *Z*-scores from these four assays.

Identifying structurally related small molecules. We used Pipeline Pilot (Scitegic) to perform *K*-means clustering of the molecules based on common and biologically intuitive chemical features (molecular weight, octanol-water partition coefficient, number of hydrogen bond donors and acceptors, and number of rotatable bonds). We set *K* to 624 to result in an average of 5 compounds per cluster. To detect enrichment for assay performance within each compound cluster, we performed the Mann-Whitney rank-sum test on each cluster in each assay.

Note: Supplementary information is available on the Nature Biotechnology website.

AUTHOR CONTRIBUTIONS
V.K.M. conceived of and supervised the project. B.K.W., T.K. and V.K.M. designed the experiments and analyzed the data. T.J.G., A.R. and B.K.W. carried out phenotypic screening. D.P. and T.K. carried out GE-HTS experiments. S.L.S. and T.R.G. provided guidance on chemical screening and GE-HTS, respectively, and advised on analysis. B.K.W., T.K. and V.K.M. wrote the paper.

1. Anderson, S. *et al.* Sequence and organization of the human mitochondrial genome. *Nature* **290**, 457–465 (1981).
2. Chance, B. & Williams, G.R. Respiratory enzymes in oxidative phosphorylation. III. The steady state. *J. Biol. Chem.* **217**, 409–427 (1955).
3. DiMauro, S. & Schon, E.A. Mitochondrial respiratory-chain diseases. *N. Engl. J. Med.* **348**, 2656–2668 (2003).
4. Mootha, V.K. *et al.* PGC-1α-responsive genes involved in oxidative phosphorylation are coordinately downregulated in human diabetes. *Nat. Genet.* **34**, 267–273 (2003).
5. Petersen, K.F. *et al.* Mitochondrial dysfunction in the elderly: possible role in insulin resistance. *Science* **300**, 1140–1142 (2003).
6. Balaban, R.S., Nemoto, S. & Finkel, T. Mitochondria, oxidants, and aging. *Cell* **120**, 483–495 (2005).
7. Kelly, D.P. & Scarpulla, R.C. Transcriptional regulatory circuits controlling mitochondrial biogenesis and function. *Genes Dev.* **18**, 357–368 (2004).
8. Weinstein, J.N. *et al.* An information-intensive approach to the molecular pharmacology of cancer. *Science* **275**, 343–349 (1997).
9. Hughes, T.R. *et al.* Functional discovery via a compendium of expression profiles. *Cell* **102**, 109–126 (2000).
10. Lamb, J. *et al.* The Connectivity Map: using gene-expression signatures to connect small molecules, genes, and disease. *Science* **313**, 1929–1935 (2006).
11. Ramanathan, A., Wang, C. & Schreiber, S.L. Perturbational profiling of a cell-line model of tumorigenesis by using metabolic measurements. *Proc. Natl. Acad. Sci. USA* **102**, 5992–5997 (2005).
12. Leary, S.C., Battersby, B.J., Hansford, R.G. & Moyes, C.D. Interactions between bioenergetics and mitochondrial biogenesis. *Biochim. Biophys. Acta* **1365**, 522–530 (1998).
13. Dolma, S., Lessnick, S.L., Hahn, W.C. & Stockwell, B.R. Identification of genotype-selective antitumor agents using synthetic lethal chemical screening in engineered human tumor cells. *Cancer Cell* **3**, 285–296 (2003).
14. Smiley, S.T. *et al.* Intracellular heterogeneity in mitochondrial membrane potentials revealed by a J-aggregate-forming lipophilic cation JC-1. *Proc. Natl. Acad. Sci. USA* **88**, 3671–3675 (1991).
15. Berridge, M.V. & Tan, A.S. Characterization of the cellular reduction of 3-(4,5-dimethylthiazol-2-yl)-2,5-diphenyltetrazolium bromide (MTT): subcellular localization, substrate dependence, and involvement of mitochondrial electron transport in MTT reduction. *Arch. Biochem. Biophys.* **303**, 474–482 (1993).
16. Crouch, S.P., Kozlowski, R., Slater, K.J. & Fletcher, J. The use of ATP bioluminescence as a measure of cell proliferation and cytotoxicity. *J. Immunol. Methods* **160**, 81–88 (1993).
17. Ye, G., Metreveli, N.S., Ren, J. & Epstein, P.N. Metallothionein prevents diabetes-induced deficits in cardiomyocytes by inhibiting reactive oxygen species production. *Diabetes* **52**, 777–783 (2003).
18. Stegmaier, K. *et al.* Gene expression–based high-throughput screening (GE-HTS) and application to leukemia differentiation. *Nat. Genet.* **36**, 257–263 (2004).
19. Peck, D. *et al.* A method for high-throughput gene expression signature analysis. *Genome Biol.* **7**, R61 (2006).
20. Kim, Y.K. *et al.* Relationship of stereochemical and skeletal diversity of small molecules to cellular measurement space. *J. Am. Chem. Soc.* **126**, 14740–14745 (2004).
21. Franz, A.K., Dreyfuss, P.D. & Schreiber, S.L. Synthesis and cellular profiling of diverse organosilicon small molecules. *J. Am. Chem. Soc.* **129**, 1020–1021 (2007).
22. Larsson, N.G. & Clayton, D.A. Molecular genetic aspects of human mitochondrial disorders. *Annu. Rev. Genet.* **29**, 151–178 (1995).
23. Clayton, D.A. Transcription of the mammalian mitochondrial genome. *Annu. Rev. Biochem.* **53**, 573–594 (1984).
24. Antonetti, D.A., Reynet, C. & Kahn, C.R. Increased expression of mitochondrial-encoded genes in skeletal muscle of humans with diabetes mellitus. *J. Clin. Invest.* **95**, 1383–1388 (1995).
25. Huang, X. *et al.* Insulin-regulated mitochondrial gene expression is associated with glucose flux in human skeletal muscle. *Diabetes* **48**, 1508–1514 (1999).
26. Heddi, A., Stepien, G., Benke, P.J. & Wallace, D.C. Coordinate induction of energy gene expression in tissues of mitochondrial disease patients. *J. Biol. Chem.* **274**, 22968–22976 (1999).
27. Graham, D.J. *et al.* Incidence of hospitalized rhabdomyolysis in patients treated with lipid-lowering drugs. *J. Am. Med. Assoc.* **292**, 2585–2590 (2004).
28. Dirks, A.J. & Jones, C.J. Statin-induced apoptosis and skeletal myopathy. *Am. J. Physiol.* **291**, C1208–C1212 (2006).
29. van Vliet, A.K., Negre-Aminou, P., van Thiel, G.C., Bolhuis, P.A. & Cohen, L.H. Action of lovastatin, simvastatin, and pravastatin on sterol synthesis and their antiproliferative effect in cultured myoblasts from human striated muscle. *Biochem. Pharmacol.* **52**, 1387–1392 (1996).
30. Frendin, T.J. & Swainson, C.P. Acute renal failure secondary to non-traumatic rhabdomyolysis following amoxapine overdose. *N. Z. Med. J.* **98**, 690–691 (1985).
31. Blessing, W. & Walsh, J.C. Myotonia precipitated by propranolol therapy. *Lancet* **309**, 73–74 (1977).

32. Davidson, B.K. Myositis associated with griseofulvin therapy. *Am. Fam. Physician* **52**, 1277 (1995).
33. Delobel, P. & Pradinaud, R. Rhabdomyolysis associated with pentamidine isethionate therapy for American cutaneous leishmaniasis. *J. Antimicrob. Chemother.* **51**, 1319–1320 (2003).
34. Rowinsky, E.K. *et al.* Phase I and pharmacologic study of paclitaxel and cisplatin with granulocyte colony-stimulating factor: neuromuscular toxicity is dose-limiting. *J. Clin. Oncol.* **11**, 2010–2020 (1993).
35. Aronson, J.K. Ed. *Meyler's Side Effects of Drugs* 15th edn. (Elsevier Science, Burlington, Massachusetts, USA, 2006).
36. Bliss, C.I. The toxicity of poisons applied jointly. *Ann. Appl. Biol.* **26**, 585–615 (1939).
37. Kelley, D.E., He, J., Menshikova, E.V. & Ritov, V.B. Dysfunction of mitochondria in human skeletal muscle in type 2 diabetes. *Diabetes* **51**, 2944–2950 (2002).
38. Houstis, N., Rosen, E.D. & Lander, E.S. Reactive oxygen species have a causal role in multiple forms of insulin resistance. *Nature* **440**, 944–948 (2006).
39. Lustbader, J.W. *et al.* ABAD directly links Aβ to mitochondrial toxicity in Alzheimer's disease. *Science* **304**, 448–452 (2004).
40. Li, W.L., Zheng, H.C., Bukuru, J. & De Kimpe, N. Natural medicines used in the traditional Chinese medical system for therapy of diabetes mellitus. *J. Ethnopharmacol.* **92**, 1–21 (2004).
41. Bonawitz, N.D., Clayton, D.A. & Shadel, G.S. Initiation and beyond: multiple functions of the human mitochondrial transcription machinery. *Mol. Cell* **24**, 813–825 (2006).
42. Wu, Z. *et al.* Mechanisms controlling mitochondrial biogenesis and respiration through the thermogenic coactivator PGC-1. *Cell* **98**, 115–124 (1999).
43. Mootha, V.K. *et al.* Errα and Gabpa/b specify PGC-1α-dependent oxidative phosphorylation gene expression that is altered in diabetic muscle. *Proc. Natl. Acad. Sci. USA* **101**, 6570–6575 (2004).
44. Valle, I., Alvarez-Barrientos, A., Arza, E., Lamas, S. & Monsalve, M. PGC-1alpha regulates the mitochondrial antioxidant defense system in vascular endothelial cells. *Cardiovasc. Res.* **66**, 562–573 (2005).
45. Freyssenet, D., Irrcher, I., Connor, M.K., DiCarlo, M. & Hood, D.A. Calcium-regulated changes in mitochondrial phenotype in skeletal muscle cells. *Am. J. Phys.* **286**, 1053–1061 (2004).
46. Caprio, S. *et al.* Improvement of metabolic control in diabetic patients during mebendazole administration: preliminary studies. *Diabetologia* **27**, 52–55 (1984).
47. Karbowski, M. *et al.* Opposite effects of microtubule-stabilizing and microtubule-destabilizing drugs on biogenesis of mitochondria in mammalian cells. *J. Cell Sci.* **114**, 281–291 (2001).
48. Mitchell, P. Coupling of phosphorylation to electron and hydrogen transfer by a chemi-osmotic type of mechanism. *Nature* **199**, 144–148 (1961).
49. Lee, P.D., Sladek, R., Greenwood, C.M. & Hudson, T.J. Control genes and variability: absence of ubiquitous reference transcripts in diverse mammalian expression studies. *Genome Res.* **12**, 292–297 (2002).
50. Hieronymus, H. *et al.* Gene expression signature-based chemical genomic prediction identifies a novel class of HSP90 pathway modulators. *Cancer Cell* **10**, 321–330 (2006).